Finite Element Modeling of Curing of Epoxy Matrix Composites

Xiangqiao Yan

Research Laboratory on Composite Materials, Harbin Institute of Technology, Harbin 150001, People's Republic of China

Received 23 November 2005; accepted 6 February 2006
DOI 10.1002/app.24337
Published online in Wiley InterScience (www.interscience.wiley.com).

ABSTRACT: A two-dimensional finite element model is developed to simulate and analyze the mechanisms pertaining to resin flow, heat transfer, and consolidation of laminated composites during autoclave processing. The model, which incorporates some of the best features of models already in existence, is based on Darcy's law, the convection–diffusion heat equation, and appropriate constitutive relations. By using a weighted residual method, a two-dimensional finite element formulation for the model is presented and a finite element code is developed. Numerical examples, including a comparison of the present numerical results with one-dimensional and two-dimensional analytical solutions, are given to indicate the accuracy the finite element formulation. Moreover, using the finite element code, the one-dimensional cure process of a laminate made of 228 and 380 plies of AS4/3501-6 unidirectional tape is simulated and numerical results are compared with available experimental results. © 2006 Wiley Periodicals, Inc. J Appl Polym Sci 103: 2310–2319, 2007

Key words: processing; flow; compaction; modeling; finite element; degree of cure

INTRODUCTION

The autoclave-assisted cure of prepreg lay-ups is an important process for fabrication of advanced polymer composites in the aerospace industry. In this process, prepreg laminae are laid on the tool surface in a prescribed fiber orientation for each layer to form the laminate. The laminate is covered with other bagging materials such as a peel ply, bleeding layer, separator, breather cloth, and vacuum bag. The entire assembly is then cured by exposing it to the prescribed temperature and pressure cure cycle. Many applications require the consolidation and curing of thick section laminates that are up to several centimeters in thickness. In consolidation processing, proper selection of the parameters, such as time, pressure, and temperature, will produce a fully compacted and cured material with good quality.

The consolidation and curing processes of polymer composites involve a simultaneous chemical reaction, resin flow, and heat transfer. Proper control of the applied consolidation pressure and temperature is necessary in order to allow the resin to flow before it gels. Resin flow is the primary mechanism for removing the excess resin and voids entrapped inside the laminate and obtaining the desired fiber volume fracture. During the process, the desired temperature cycle is applied at the surface of the laminate to heat the entire laminate assembly. The temperature at the center of the laminate tends to increase more slowly than the applied surface temperature because of the low heat conductivity of the laminate and then rises to a higher value because of the resin exotherm. The high temperature overshoot at the center areas sometimes causes the problem of a runaway thermal reaction, resulting in material degradation. In addition, an uneven temperature history across the thickness will result in uneven cure and residual stresses.

These difficulties in the consolidation and curing process are aggravated in the fabrication of thick composite laminates. Major temperature lag and overshoot at the center of a laminate is usually experienced because of the large thickness and low thermal conductivity of the composite. Furthermore, it also requires a longer time for the resin bleed out of the laminate. In some cases, consolidation cannot be completed before the resin viscosity rises beyond the processable range, which results in a poor consolidation region in the core area. Proper design of the cure cycle can reduce the problem of temperature overshoot during the process. As for the degree of consolidation, analyses of both the resin cure and compacting processes are required. This article addresses the effect of the compacting pressure and cure cycle on the consol-

Correspondence to: X. Yan (yanxiangqiao@hotmail.com).
Contract grant sponsor: National Natural Science Foundation of China; contract grant number: 10272037.

idation of thick laminates based on cure and compacting simulation models.

Background

Numerous studies have been directed at the modeling and simulation of various aspects of the consolidation and cure of composite laminates,[1–17] including resin flow, cure kinetics, and void growth. Loos and Springer[1] developed a model that assumed pressure gradients in both the vertical and horizontal directions, but they computed the flow separately in the two directions. They described the vertical flow in the laminate in terms of Darcy's law for flow through porous media and assumed the horizontal flow as a viscous flow between two parallel plates. Other studies[2–4] computed the horizontal flow on the basis of Darcy's law and proposed models to determine the load carried by the fibers during the consolidation of the laminate. Gutowski et al.[5] subsequently proposed a general mathematical model, which allowed for three-dimensional flow and one-dimensional consolidation of the composite. The resin flow was modeled by using Darcy's law for an anisotropic porous medium. They carried out a two-dimensional flow analysis of the compression molding and a one-dimensional analysis through thickness consolidation. Dave et al.[6] employed Darcy's law to model the consolidation process in both the vertical and horizontal directions. Dave et al.[7] also described a general flow model for resin flows in fiber reinforcements, which led to a consolidation flow model similar to that proposed by Gutowski et al.[5] Young[10] generalized the three-dimensional consolidation model to include the cases of angle or cross-ply laminates and a nonplanar composite laminate. Ciricioli et al.[9] performed experimental measurements of the prepreg consolidation process. Their results could be used to compare with the simulation results of the consolidation model.

This article describes a two-dimensional finite element model developed to simulate and analyze the mechanisms dealing with resin flow, heat transfer, and consolidation of laminated composites during autoclave processing. The model, which incorporates some of the best features of models already reported in the literature, is based on the Darcy law, the convection–diffusion heat equation, and appropriate constitutive relations. By using a weighted residual method, two-dimensional finite element formulation for the model is presented and the finite element code is developed. Numerical examples, including a comparison of the present numerical results with one-dimensional and two-dimensional analytical solutions, are given to indicate the accuracy of the finite element formulation. Using the finite element code, the one-dimensional cure process of a laminate made of 228 and 380 plies of AS4/3501-6 unidirectional tape is simulated and numerical results are compared with experimental results available in the literature.

EXPERIMENTAL

Consolidation model

During the consolidation of a laminated composite, pressure is applied at a specific time. The applied pressure is shared by the resin and fiber of the laminate simultaneously. The consolidation pressure taken by the resin will drive the resin to flow out of the laminate in directions both normal and parallel to the tool surfaces, and the flow rate depends on the resin viscosity and fiber permeability. The fiber permeability decreases during the consolidation process whereas the fiber volume fraction increases. Because the fiber acts as a nonlinear spring,[4,5] the laminate thickness gradually deceases and more and more consolidation pressure is taken by the fiber. At the end of consolidation, the applied pressure is completely supported by the fibrous bed if gelation does not occur before that time. Because the applied load is shared by the resin and fibrous bed, the force equilibrium equation can be written as[6]

$$\sigma = p + P \tag{1}$$

where σ is the total externally applied stress, p is the effective stress (i.e., the stress borne by the springlike skeletal structure of the porous bed), and P is the hydraulic pressure of the resin in the porous medium.

The equation of the resin flow during the consolidation process is expressed as[8]

$$-m_v \frac{\partial P}{\partial t} + \frac{\partial}{\partial x}\left(\frac{k_x}{\mu}\frac{\partial P}{\partial x}\right) + \frac{\partial}{\partial y}\left(\frac{k_y}{\mu}\frac{\partial P}{\partial y}\right) = 0 \tag{2}$$

where k_x and k_y are the fiber permeability in the direction of the fiber and perpendicular to the fiber direction, respectively; μ is the viscosity of the resin; and m_v is the coefficient of volume compressibility,[8] which is

$$m_v = -\frac{1}{1+e}\frac{de}{dp} \tag{3}$$

in which e is the void rate (volume of voids/unit volume of solid fiber in the laminate),

$$e = \frac{1 - V_f}{V_f} \tag{4}$$

where V_f is the fiber volume content of composites. The value of de/dp in eq. (3) can be obtained from the stress–strain relationship of the porous fiber network. In the actual consolidation process, the void ratio of the laminate will vary according to the change of the

effective stress. One relation used in the following simulations between the effective stress and the void ratio was derived by Young[11] from the consolidation experiments conducted by Gutowski et al.:[4]

$$e = \begin{cases} -1.552 \times 10^{-6}\, p + 0.81 & \text{for} \quad 0 \le p \le 68.95 \times 10^3 Pa \\ -0.247 \log_{10} p + 1.899 & \text{for} \quad p \le 68.95 \times 10^3 Pa \end{cases} \tag{5}$$

The k_x and k_y used in the following simulations is given by[18,19]

$$k_x = \frac{r_f^2(\pi + 2.15V_f)(1 - V_f)}{48V_f^2},$$

$$k_y = \frac{r_f^2(1 - V_f^*)\left(1 - \sqrt{V_f^*}\right)^2}{24(V_f^*)^{1.5}} \tag{6}$$

where

$$V_f^* = \begin{cases} V_f, & V_f \ge 0.5, \\ 2.2V_f^2 - 1.22V_f + 0.56, & V_f \ge 0.5 \end{cases}$$

The boundary conditions of eq. (2) can be classified as[17]

$$\frac{\partial P}{\partial n} = 0, \quad x, y \subset \Gamma_2 \tag{7}$$

$$q_n = h(P - P_a), \quad x, y \subset \Gamma_3 \tag{8}$$

where P_a is the environment pressure and h is an effective flow coefficient. It is obvious that the boundary conditions expressed in terms of eqs. (7) and (8) are similar to insulation and convection boundary conditions, respectively, in heat transfer analysis. In view of this, the insulation boundary condition in heat transfer analysis can be treated as a convection boundary condition by letting the effective convection heat transfer coefficient h be equal to zero. Thus, in this formulation, only the boundary condition expressed in terms of eq. (8) is considered.

By using Darcy's law for fluid flow through an orthotropic material, whose coordinate axes are aligned with the principal axes of material, we find

$$q_i = -\frac{k_i}{\mu}\frac{\partial P}{\partial x_i} \tag{9}$$

Then, boundary condition (8) can be rewritten as

$$q_n = q_x n_x + q_y n_y = -\frac{k_x}{\mu}\frac{\partial P}{\partial x} n_x - \frac{k_y}{\mu}\frac{\partial P}{\partial y} n_y = h(P - P_a) \tag{10}$$

where n_x and n_y are the normal directional cosines on boundaries.

Thermochemical model

During the autoclave processing of composite materials, the temperature is assumed to be in local equilibrium at any time because of its slow processing speed. The two-dimensional heat transfer differential equation is expressed as

$$\rho c \frac{\partial T}{\partial t} + \rho_r c_r \left[\frac{\partial}{\partial x}(uT) + \frac{\partial}{\partial y}(wT)\right] - \frac{\partial}{\partial x}\left(\lambda_{xx}\frac{\partial T}{\partial x}\right) - \frac{\partial}{\partial y}\left(\lambda_{yy}\frac{\partial T}{\partial y}\right) - Q = 0 \tag{11}$$

where Q is an interior heat source; ρ and c are the density and specific heat of a composite material, respectively; ρ_r and c_r are the density and specific heat of a resin, respectively; u and v are the resin flow speeds in the x and y directions, respectively; and t is time.

The boundary conditions of eq. (11) are

$$T(x, y) = T_c(x, y, t) \tag{12}$$

$$\lambda_{xx}\frac{\partial T}{\partial x} n_x + \lambda_{yy}\frac{\partial T}{\partial y} n_y = v_a(x, y, t), \quad x, y \subset \Gamma_2 \tag{13}$$

$$\lambda_{xx}\frac{\partial T}{\partial x} n_x + \lambda_{yy}\frac{\partial T}{\partial y} n_y = h_T(T_a - T), \quad x, y \subset \Gamma_3 \tag{14}$$

where Γ_1, Γ_2, and Γ_3 are the first, second, and third boundary conditions, respectively; T_c (x, y, t) is a known boundary temperature function; v_a (x, y, t) is a known boundary heat current density function, in which it is positive when heat is fluidized into the body we studied; h_T is a boundary transfer coefficient; and T_a is a circumstance temperature.

It is generally assumed that the thermal conductive properties of composite materials are uniform and transversely isotropic and are characterized by means of the longitudinal (λ_{xx}) and transverse (λ_{yy}) thermal conductive coefficients. Based on the weight-average rule, the heat capacity (c), density (∂), and λ_{xx} parameters in eq. (11) are determined. The λ_{yy} in eq. (11) is calculated using the Springer–Tsai model,[20]

$$\frac{\lambda_{yy}}{\lambda_{xx}} = \left(1 - 2\sqrt{\frac{V_f}{\pi}}\right) + \frac{1}{B}\left[\pi - \frac{4}{\sqrt{1 - \frac{B^2 V_f}{\pi}}}\tan^{-1}\frac{\sqrt{1 - \frac{B^2 V_f}{\pi}}}{1 + B\sqrt{\frac{V_f}{\pi}}}\right] \tag{15}$$

where $B = 2(\lambda_r/\lambda_f - 1)$, V_f is the fiber volume fraction, λ_r is the conductivity of the resin, and λ_f is the conductivity of the fiber.

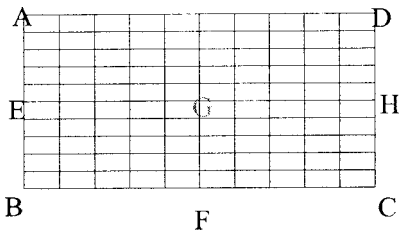

Figure 1 A finite element mesh (including typical points).

The resin kinetics are those proposed in Lee et al.[21] The internal heat generation in eq. (11) is

$$Q = \rho_r V_r H_R \frac{d\alpha}{dt} \tag{16}$$

where the rate of cure is

$$\frac{d\alpha}{dt} = \begin{cases} (K_1 + K_2\alpha)(1-\alpha)(0.47-\alpha), & \alpha \le 0.3 \\ K_3(1-\varepsilon), & \alpha \le 0.3 \end{cases} \tag{17}$$

in which

$$K_i = A_i \exp\left(\frac{-E_i}{RT}\right), \quad i = 1,\ 2,\ 3 \tag{18}$$

where H_R is the total heat of reaction; A_1, A_2, and A_3 are preexponential factors; E_1, E_2, and E_3 are activation energies; and R is the universal gas constant.

The resin viscosity proposed by Lee et al.[21] is also used:

$$\mu = \mu_\infty \exp\left(\frac{U}{RT} + K_\mu \alpha\right) \tag{19}$$

where U is the activity energy and K_μ is a constant.

Finite element formulation

Because the control equations in the consolidation model are similar to those in the thermochemical model, here, finite element formulations are given only for the thermochemical model. However, a finite element code developed in this article is a united code, which combines the consolidation model with the thermochemical model. Using the two-dimensional heat transfer differential equation [eq. (11)], boundary conditions [eqs. (12)–(14)], and a weight residual method,[22] a two-dimensional finite element formulation is presented.

According to the finite element method, the regime (Ω) is separated into finite elements and the pressure field function (T) in each element is interpolated by its nodal temperature (T_i)

$$T = \sum_{i=1}^{n^e} N_i(x,y) T_i = N \times T^e \tag{20}$$

in which

$$N = [N_1, N_2, \ldots, N_{n^e}] \tag{21}$$

$$T^e = [T_1, T_2, \ldots, T_{n^e}]^T \tag{22}$$

where n^e is the number of nodes in an element and $N_i(x,\ y)$ is the interpolation function corresponding to node i.

Introducing the following symbols,

$$K^e_{ij\lambda} = \int_{\Omega^e} \left[\frac{\partial N_i}{\partial x}\left(\lambda_{xx}\frac{\partial N_j}{\partial x}\right) + \frac{\partial N_i}{\partial y}\left(\lambda_{yy}\frac{\partial N_j}{\partial y}\right)\right] d\Omega \tag{23}$$

$$K^e_{ijh} = \int_{\Gamma^e_3} h_T N_i N_j d\Gamma \tag{24}$$

$$K^e_{ijuv} = \int_{\Omega^e} \rho_r c_r \left(\frac{\partial u}{\partial x} + \frac{\partial v}{\partial y}\right) N_i N_j d\Omega \tag{25}$$

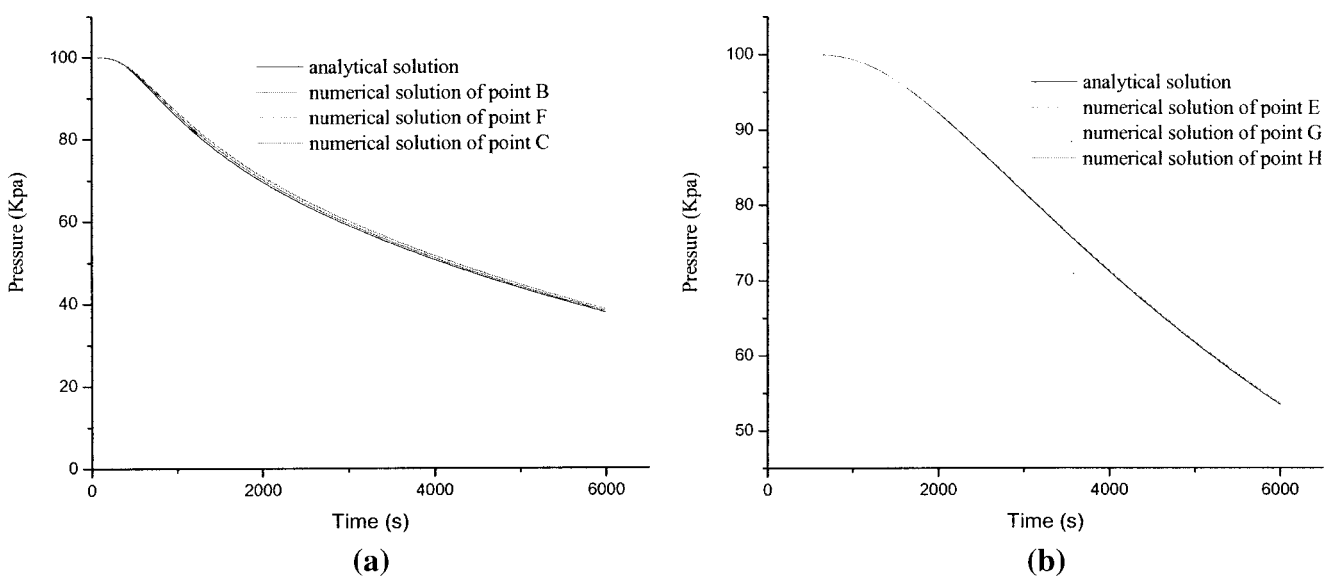

Figure 2 A comparison of the numerical and analytical results for a one-dimensional case.

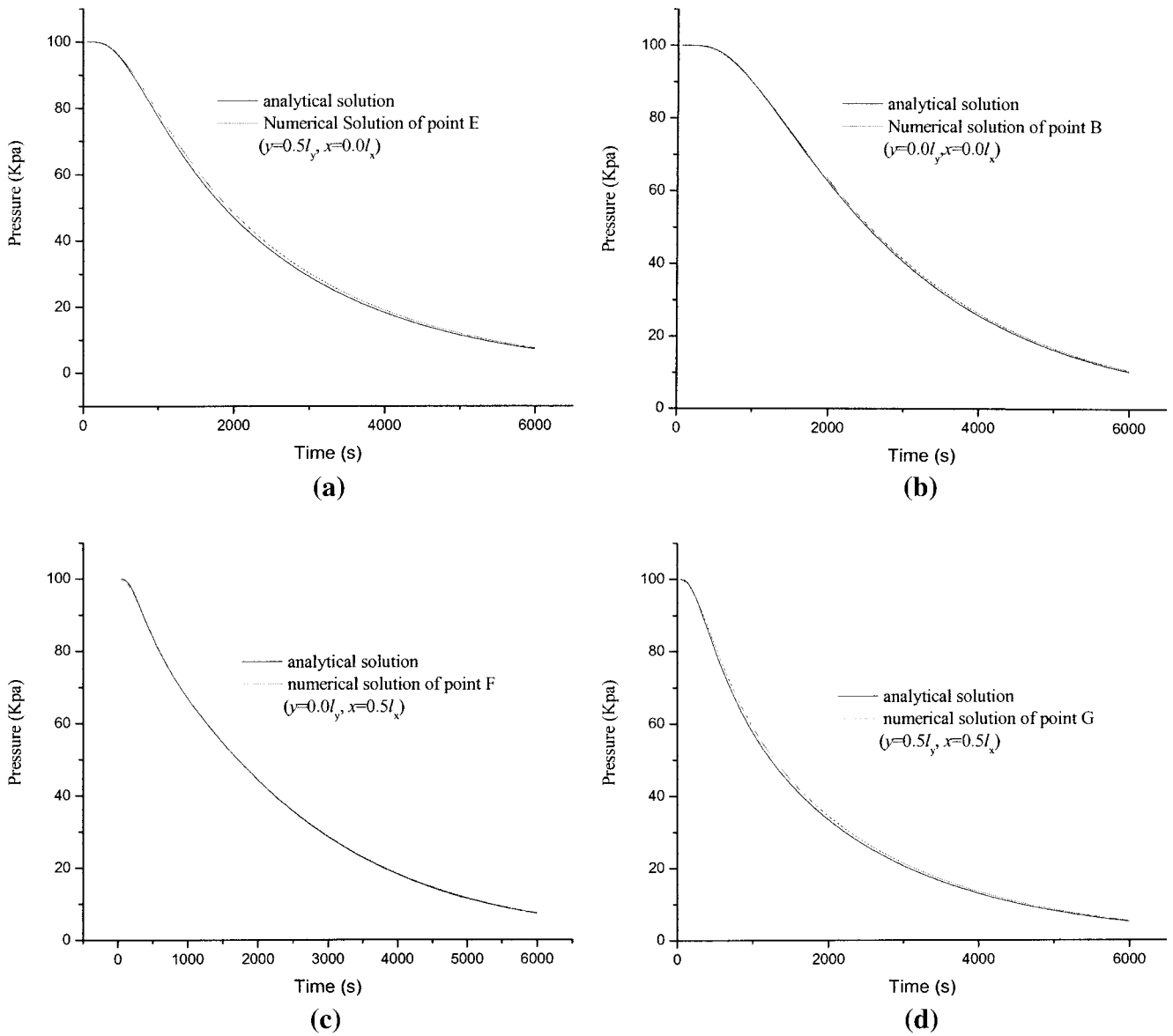

Figure 3 A comparison of the numerical and analytical results for a two-dimensional case.

$$K^e_{iju} = \int_{\Omega^e} \rho_r c_r u \frac{\partial N_i}{\partial x} N_j d\Omega \tag{26}$$

$$K^e_{ijv} = \int_{\Omega^e} \rho_r c_r v \frac{\partial N_i}{\partial y} N_j d\Omega \tag{27}$$

$$F^e_{\Gamma_{3i}} = \int_{\Gamma^e_3} h_T T_a N_i d\Gamma \tag{28}$$

$$F^e_{\Gamma_{2i}} = \int_{\Gamma^e_2} v_a N_i d\Gamma \tag{29}$$

$$F^e_{Qi} = \int_{\Omega^e} Q N_i d\Omega \tag{30}$$

$$C^e_{ij} = \int_{\Omega^e} \rho c N_i N_j d\Omega \tag{31}$$

finite element equations corresponding to eqs. (11)–(14) can be expressed as

$$CT + KT = F \tag{32}$$

where

$$K_{ij} = \sum_e (K^e_{ij\lambda} + K^e_{ijh} + K^e_{ijuw} + K^e_{iju} + K^e_{ijw}) \tag{33}$$

$$F_i = \sum_e (F^e_{\Gamma_2 i} + F^e_{\Gamma_3 i} + F^e_{Qi}) \tag{34}$$

$$C_{ij} = \sum_e C^e_{ij} \tag{35}$$

Here, $\sum_e$ indicates the sum for all elements.

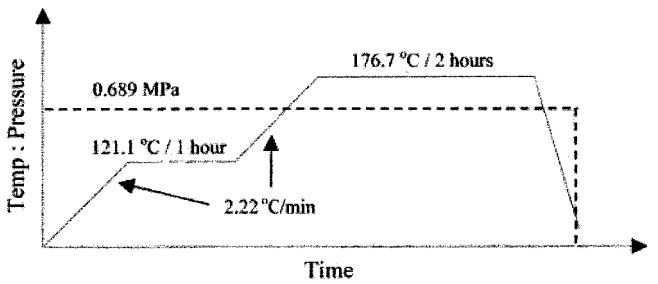

Figure 4 The cure cycle.

Numerical validation verification

Using the finite element formulation of a resin flow during the autoclave processing of composite materials, a finite element code is developed in this investigation. In this code, a quadrilateral element with four nodes and a backward difference formula for a time t are used.

In order to illustrate the accuracy and efficiency of the finite element formulation presented in the previous section, it is assumed here that the parameters k_x ($=6.45 \times 10^{-12}$ m^2), k_y($=6.45 \times 10^{-13}$ m^2), m_v($=8.7025 \times 10^{-7}$ Pa^{-1}), μ (=100 P), and, and the laminate thickness ($0.1524 \times 0.1524 \times 0.03556$ m) are constants during the consolidation process. This is because analytical closed form solutions are currently available for one-dimensional and two-dimensional problems.

TABLE I
Parameters Used in Cure Simulation of AS4/3501-6 Graphite/Epoxy Laminate

Parameters of resin kinetics	
Preexponential factor	
A_1 (min^{-1})	2.101×10^9
A_2 (min^{-1})	-2.014×10^9
A_3 (min^{-1})	1.960×10^5
Activity energy	
E_1 (J/mol)	8.07×10^4
E_2 (J/mol)	7.78×10^4
E_3 (J/mol)	5.56×10^4
Parameters of viscosity model	
Viscosity constant (Pa s)	7.93×10^{-14}
Activity energy for viscosity (J/mol)	9.08×10^{10}
Viscosity constant	14.1
Other parameters	
Fiber	
Radius (m)	3.5×10^{-6}
Volume fraction (%)	50
Density	1.79×10^3 kg/m^3
Resin density	1.26×10^3 kg/m^3
Specific heat	
Fiber	7.12×10^2 J/(kg K)
Resin	1.26×10^2 J/(kg K)
Thermal conductivity	
Fiber	26 W/(m K)
Resin	0.167 W/(m K)

The parameters are according to Lee et al.[21]

Example 1: One-dimensional comparison

In this subsection, we consider a two-dimensional unidirectional laminate with dimensions of 0.0762 $\times$ 0.03556 m, whose pressure boundary conditions are $\partial P/\partial n = 0$ for the bottom surface (boundary BC, Fig. 1), $\partial P/\partial n = 0$ for the side surfaces (boundaries AB and CD, Fig. 1), and $P = 0$ Pa (bag pressure) for the top surface (boundary AD, Fig. 1), and whose initial pressure condition (P_0) is 100 kPa. Obviously, the transient pressure fields in the laminate are one dimensional, that is, $P = P(y, t)$. An analytical solution for this problem can be obtained by using formula (4–25) in Eckert and Drake,[23] which is

$$P(y,t) = \frac{4P_0}{\pi} \sum_{j=0}^{\infty} \frac{(-1)^j}{(2j+1)} \cos\left[\frac{(2j+1)\pi y}{2l_y}\right] \times \exp\left\{\frac{(2j+1)^2\pi^2\alpha_y t}{4{l_y}^2}\right\} \quad (36)$$

where $\alpha_y = k_y/\eta m_v$ and l_y is the length of the y direction of the laminate ($l_y = 0.03556$ m).

Using the finite element code developed in this investigation, a numerical analysis for this transient pressure transfer problem was carried out. Figure 1 shows a finite element mesh with 121 nodes and 100 elements. Figure 2(a) provides a transient pressure comparison between analytical [$y = 0$ m is taken in formula (36)] and numerical solutions for points B($x = 0$ m, $y = 0$ m), F($x = 0.0762/2$ m, $y = 0$ m), and C($x = 0.0762$ m, $y = 0$ m). Figure 2(b) gives a transient pressure comparison between analytical [$y = 0.03556/2$ m is assumed in formula (36)] and numerical solutions for points E($x = 0$ m, $y = 0.03556/2$ m), G($x = 0.0762/2$ m, $y = 0.03556/2$ m), and H($x = 0.0762$ m,

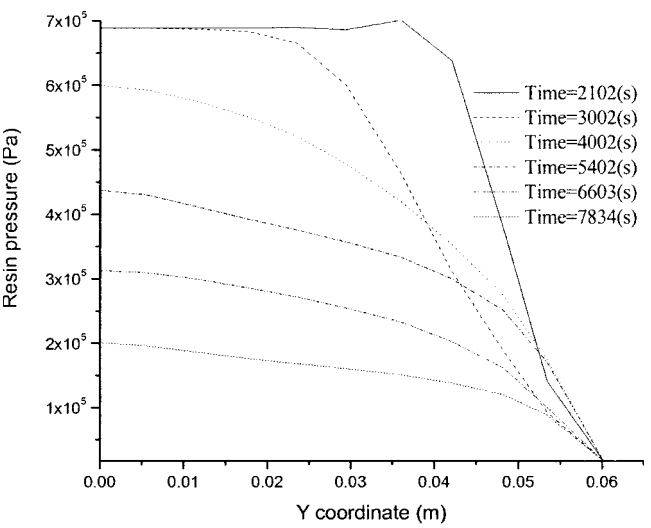

Figure 5 The variation of the resin pressure along the laminate thickness with the cure time for 380-ply unidirectional tape.

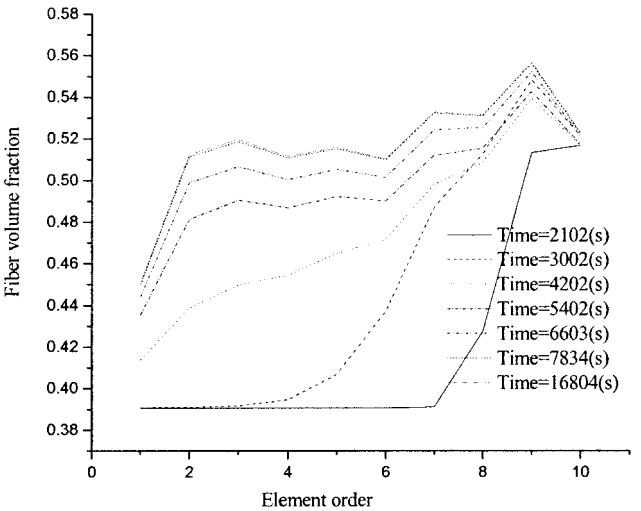

Figure 6 The variation of the fiber volume fraction along the laminate thickness with the cure time for 380-ply unidirectional tape.

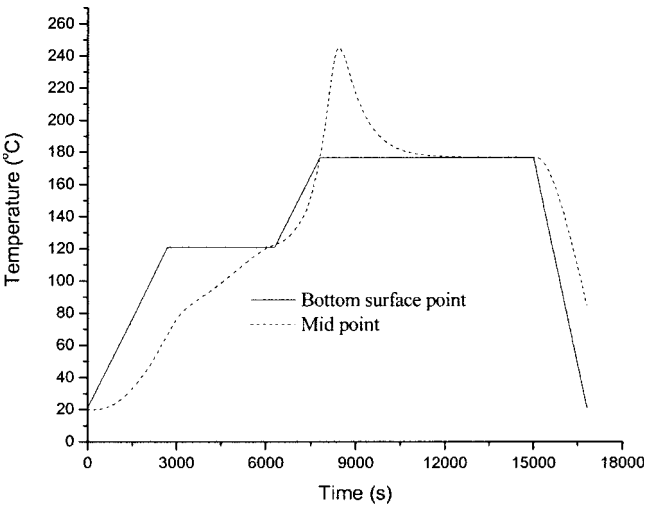

Figure 8 A comparison of the temperature between the bottom surface point and midpoint for 380-ply unidirectional tape.

$y = 0.03556/2$ m). Figure 2 shows that the transient pressure fields in the laminate are indeed one dimensional and the agreement between the analytical and numerical solutions is excellent.

Example 2: Two-dimensional comparison

Here, we consider a two-dimensional unidirectional laminate with dimensions of 0.0762 × 0.03556 m, whose pressure boundary conditions are $\partial P/\partial n = 0$ for the bottom surface (boundary *BC*, Fig. 1), $\partial P/\partial n = 0$ for the left side surface (boundary *AB*, Fig. 1), and $P = 0$ Pa for the right and top surfaces (boundaries *CD* and *AD*, Fig. 1), and whose P_0 value is 100 kPa. Obviously, the transient pressure fields in the laminate are two dimensional, that is, $P = P(x, y, t)$. An analytical solution for this problem can be obtained by using formulas (4–25), (4–49), and (4–52) in Eckert and Drake,[23]

$$\frac{P(x,y,t)}{P_0} = \frac{16}{\pi^2}\sum_{q=0}^{\infty}\sum_{j=0}^{\infty}\frac{(-1)^j}{(2j+1)}\cdot\frac{(-1)^q}{(2q+1)} \times \cos\left[\frac{(2j+1)\pi x}{2l_x}\right]\cdot\cos\left[\frac{(2q+1)\pi y}{2l_y}\right] \times \exp\left\{-\left[\frac{(2j+1)^2\pi^2\alpha_x}{4{l_x}^2}+\frac{(2q+1)^2\pi^2\alpha_y}{4{l_y}^2}\right]t\right\} \quad (37)$$

where $\alpha_x = k_x/\eta m_v$, $\alpha_y = k_y/\eta m_v$, and l_x and l_y are the lengths in the respective x and y directions of a two-dimensional geometry body ($l_y = 0.03556$ m, $l_x = 0.0762$ m).

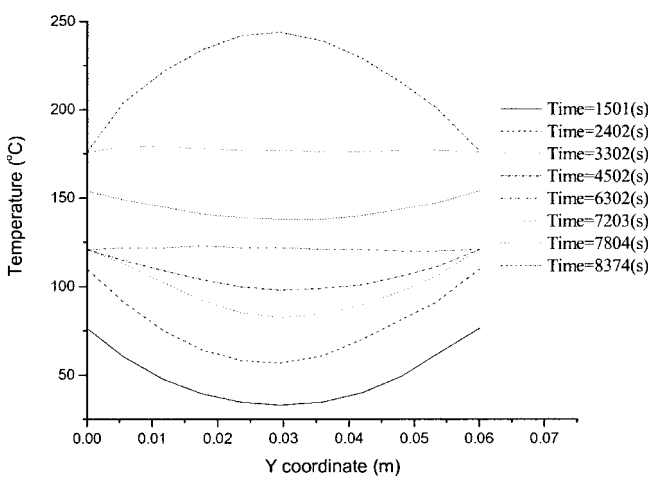

Figure 7 The variation of the temperature along the laminate thickness with the cure time for 380-ply unidirectional tape.

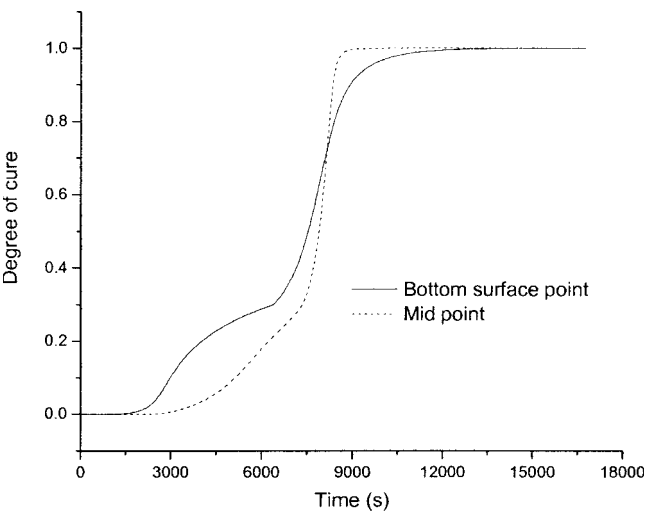

Figure 9 A comparison of the degree of cure between the bottom surface point and midpoint for 380-ply unidirectional tape.

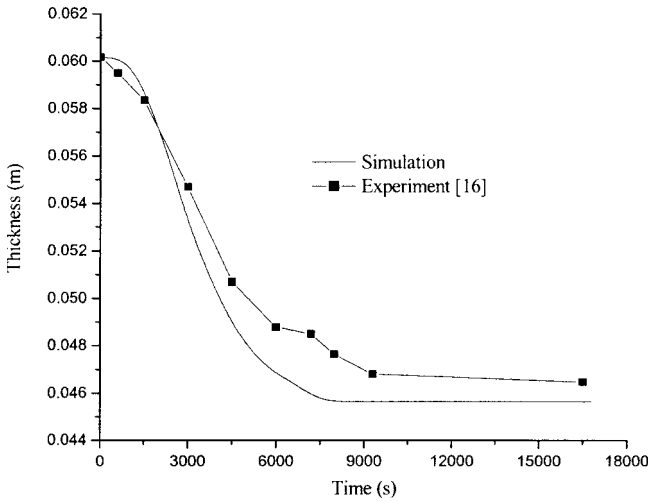

Figure 10 The variation of the thickness with the cure time for 380-ply unidirectional tape.

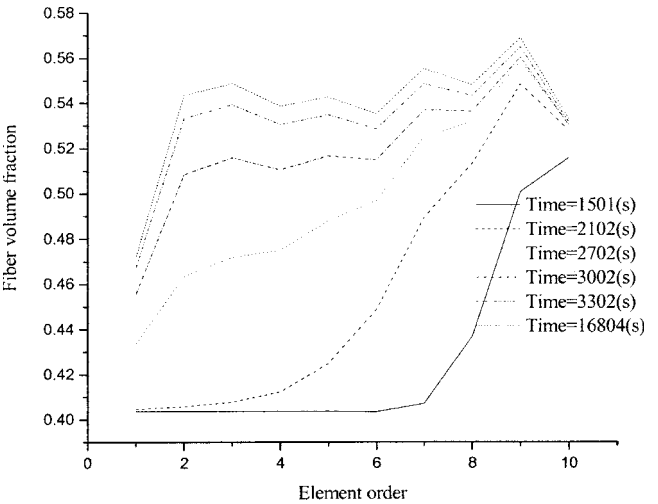

Figure 12 The variation of the fiber volume fraction along the laminate thickness with the cure time for 228-ply unidirectional tape.

Using the finite element code developed in this investigation, a numerical analysis for this transient pressure transfer problem was performed. The finite element mesh used in this analysis is shown in Figure 1. Figure 3(a–d) provides transient pressure comparisons between analytical and numerical solutions for points $E(x = 0$ m, $y = 0.03556/2$ m), $B(x = 0$ m, $y = 0$ m), $F(x = 0.0762/2$ m, $y = 0$ m), and $G(x = 0.0762/2$ m, $y = 0.03556/2$ m). Note from Figure 3 that the transient pressure fields in the laminate are confirmed to be two dimensional and the agreement between the analytical and numerical solutions is excellent as well.

RESULTS AND DISCUSSION

The finite element code, which combines the consolidation model with the thermochemical model during the autoclave processing of composite materials, is used in this section to simulate the one-dimensional cure process of a laminate made of 380- and 228-ply AS4/3501-6 unidirectional tapes. The tapes have uncompacted thicknesses and initial fiber volume fractions of 6.018 cm and 39.074% for the former and 3.576 cm and 40.383% for the latter. Further, simulation results are compared with the experimental results reported in Shin and Han.[16] Figure 4 shows its cure cycle. The pressure in the bleeder is 16.7 kPa, which is typical of the bleeder pressure in commercial composite processing using vacuum bagging procedures.[1] The material parameters required in this simulation for the AS4/3501-6 unidirectional tape are listed in Table I.

For the 380-ply AS4/3501-6 unidirectional tape, the variations of the resin pressure and fiber volume frac-

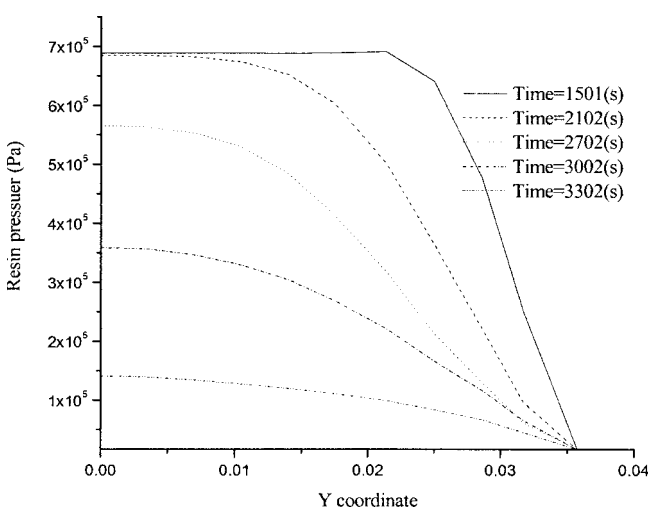

Figure 11 The variation of the resin pressure along the laminate thickness with the cure time for 228-ply unidirectional tape.

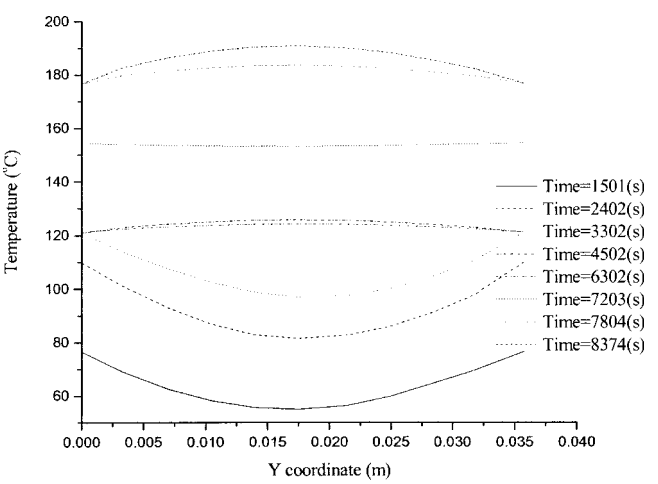

Figure 13 The variation of the temperature along the laminate thickness with the cure time for 228-ply unidirectional tape.

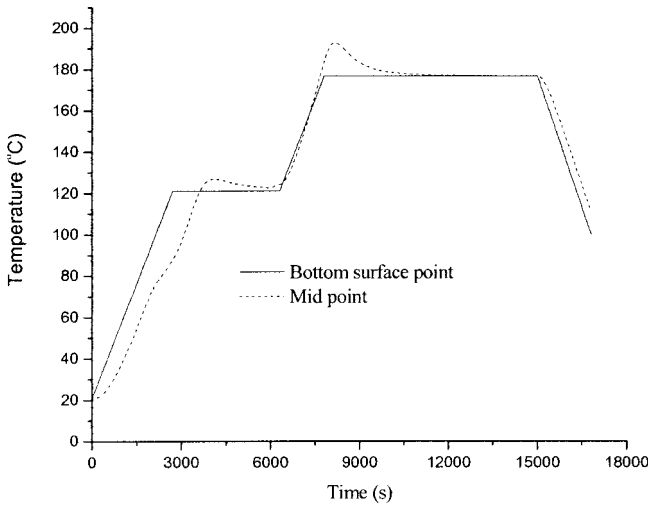

Figure 14 A comparison of the temperature between the bottom surface point and midpoint for 228-ply unidirectional tape.

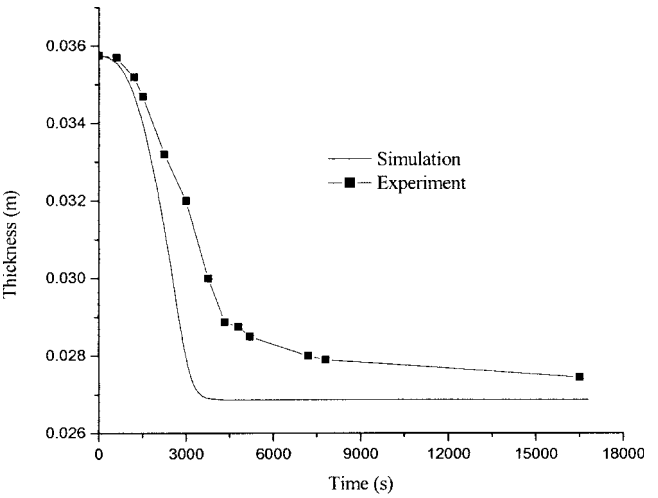

Figure 16 The variation of the thickness with the cure time for 228-ply unidirectional tape.

tion along the laminate thickness with the cure time are provided in Figures 5 and 6, respectively. Figure 7 gives the variation of the temperature along the laminate thickness with the cure time. Figures 8 and 9 show a comparison of the temperature and degree of cure between the bottom surface point and midpoint. Figure 10 pictures the variation of the thickness with the cure time, including the numerical simulation and experimental results, in which the experimental and simulation results of the compacted thickness are 4.648 and 4.564 cm, respectively.

For the 228-ply AS4/3501-6 unidirectional tape, the variations of the resin pressure and fiber volume fraction along the laminate thickness with the cure time are demonstrated in Figures 11 and 12, respectively. Figure 13 shows the variation of the temperature along the laminate thickness with the cure time. Figures 14 and 15 provide a comparison of the temperature and degree of cure between the bottom surface point and midpoint. The variation of the thickness with the cure time, including the numerical simulation and experimental results, in which the experimental and simulation values of the compacted thickness are 2.745 and 2.686 cm, respectively, are presented in Figure 16.

Figures 7, 8, 13, and 14 show that the temperature variation feature along the laminate thickness in the thick and thin composites is the same as that reported in Loos and Springer.[1]

We find from Figures 5 and 11 that the variation of the resin pressure near the bleeder in the thick and thin composites with the cure time has a slightly different tendency (see also Fig. 17).

Figures 10 and 16 show that the present numerical results of the variation of the laminate thickness with

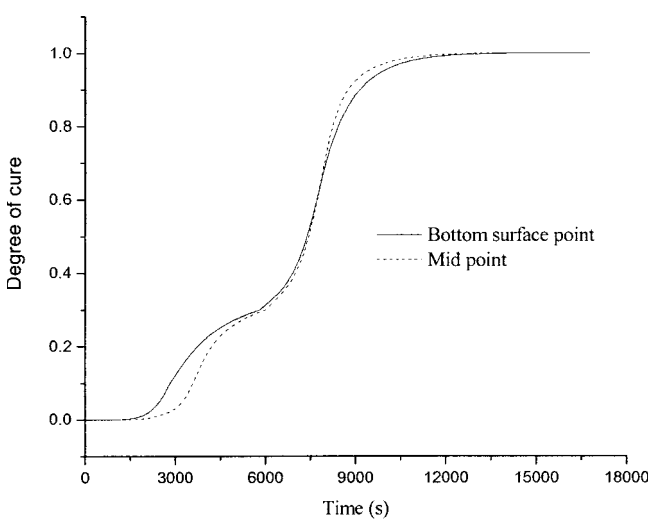

Figure 15 A comparison of the degree of cure between the bottom surface point and midpoint for 228-ply unidirectional tape.

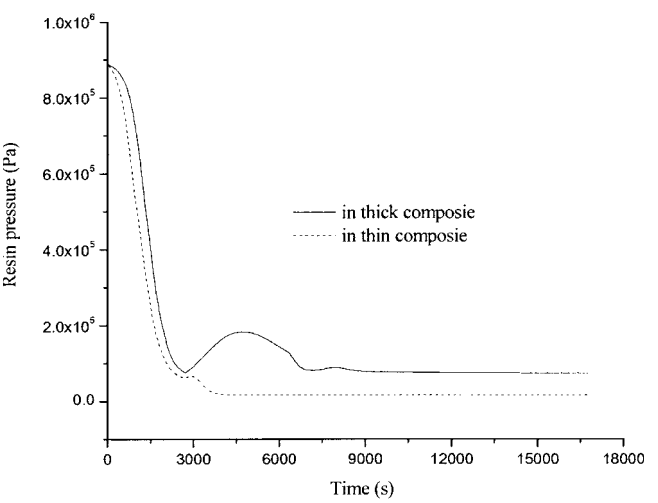

Figure 17 A comparison of the resin pressure near the bleeder in the thick and thin composites with the cure time.

the cure time are in excellent agreement with the experimental results.[16]

CONCLUSIONS

This article described a two-dimensional numerical model developed to simulate and analyze the mechanisms dealing with resin flow, heat transfer, and consolidation of laminated composites during autoclave processing. Numerical examples, including a comparison of the present numerical results with one-dimensional and two-dimensional analytical solutions, were given to indicate the accuracy of the numerical model. A numerical model was used to simulate the one-dimensional cure process of a laminate made of 228- and 380-ply AS4/3501-6 unidirectional tape, and numerical results were compared with experimental results available in the literature.

The author expresses special thanks to the National Natural Science Foundation of China for supporting this work.

References

1. Loos, A. C.; Springer, G. S. J Compos Mater 1983, 17, 135.
2. Gutowski, T. G. SAMPE Q 1985, 16, 58.
3. Gutowski, T. G.; Cai, Z.; Kingery, J.; Wineman, S. J. SAMPE Q 1986, 17, 54.
4. Gutowski, T. G.; Cai, Z.; Bauer, S.; Boucher, D. J Compos Mater 1987, 21, 172.
5. Gutowski, T. G.; Morigaki, T.; Cai, Z. J Compos Mater 1987, 21, 650.
6. Dave, R.; Kardos, J. L.; Dudukovie, M. P. Polym Compos 1987, 8, 29.
7. Dave, R.; Kardos, J. L.; Dudukovie, M. P. Polym Compos 1987, 8, 123.
8. Dave, R. J Compos Mater 1990, 24, 22.
9. Ciricioli, P. R.; Wang, Q.; Springer, G. S. J Compos Mater 1992, 26, 90.
10. Young, W. B. Polym Compos 1995, 16, 250.
11. Young, W. B. Polym Compos 1996, 17, 142.
12. Susich, D. F.; Laananen, D. H.; Ruffner, D. Compos Manufact 1993, 4, 139.
13. White, S. R.; Hahn, H. T. J Compos Mater 1993, 27, 1352.
14. Kenny, J. M. Compos Struct 1994, 27, 129.
15. Bogetti, T. A.; Gillespie, J. W. J Compos Mater 1991, 25, 239.
16. Shin, D. D.; Hahn, H. T. Polym Compos 2004, 25, 49.
17. Naji, M. I.; Hoa, S. Y. J Compos Mater 2000, 34, 1710.
18. der Westthuizen, J. V.; Du Plessis, J. P. Composites 1996, 27A, 263.
19. der Westthuizen, J. V.; Du Plessis, J. P. J Compos Mater 1994, 28, 619.
20. Springer, G. S. S.; Tsai, W. J Compos Mater 1967, 1, 166.
21. Lee, W. I.; Loos, A. C.; Springer, G. S. J Compos Mater 1982, 16, 510.
22. Zienkiewicz, O. C. The Finite Element Method; McGraw–Hill: New York, 1977.
23. Eckert, E. R. G.; Drake, R. M. Analysis of Heat and Mass Transfer; McGraw–Hill: New York, 1972.